infrastructures

Article

Exploring the Effect of Near-Field Ground Motions on the Fragility Curves of Multi-Span Simply Supported Concrete Girder Bridges

Hassan Soltanmohammadi [1], Mohammadreza Mashayekhi [1], Mohammad Mahdi Memarpour [2], Denise-Penelope N. Kontoni [3,4,*] and Masoud Mirtaheri [1]

[1] Department of Civil and Environmental Engineering, K.N. Toosi University of Technology, Tehran P.O. Box 34157-85749, Iran; hassan.soltanmohammadi@email.kntu.ac.ir (H.S.); m.mashayekhi@kntu.ac.ir (M.M.); mmirtaheri@kntu.ac.ir (M.M.)
[2] Department of Civil Engineering, Faculty of Engineering and Technology, Imam Khomeini International University, Qazvin P.O. Box 34149-16818, Iran; memarpour@eng.ikiu.ac.ir
[3] Department of Civil Engineering, School of Engineering, University of the Peloponnese, GR-26334 Patras, Greece
[4] School of Science and Technology, Hellenic Open University, GR-26335 Patras, Greece
* Correspondence: kontoni@uop.gr or kontoni.denise@ac.eap.gr

Abstract: Investigating the impact of near-field ground motions on the fragility curves of multi-span simply supported concrete girder bridges is the main goal of this paper. Fragility curves are valuable tools for evaluating seismic risks and vulnerabilities of bridges. Numerous studies have investigated the impact of ground motions on the fragility curves of bridges. Ground motions are commonly categorized into two sets, based on the distance of the recorded station from the seismic source: far-field and near-field. Studies examining the influence of near-field records on bridge fragility curves vary depending on the specific bridge type and type of fragility curve being analyzed. Due to the widespread use of multi-span simply supported concrete girder bridges in the Central and Southeastern United States, this study makes use of this bridge type. This research investigates the component fragility curves for column curvatures, bearing deformations, and abutment displacements by employing 3-D analytical models and conducting nonlinear time history analysis. These curves illustrate the impact of near-field ground motions on different components. The component fragility curves for two sets of records, 91 near-field ground motions and 78 far-field ground motions, were obtained and compared. These findings demonstrate that near-field ground motions have a greater damaging effect on columns and abutments than far-field earthquakes. When it comes to bearing deformations, the far-field earthquake impact is more severe at lower intensities, whereas the impact of the near-field ground motion is stronger at higher intensities.

Keywords: vulnerability assessment; near-fault ground motion; analytical fragility curve; nonlinear time history analysis; column curvature; girder bridge; abutment displacement

Citation: Soltanmohammadi, H.; Mashayekhi, M.; Memarpour, M.M.; Kontoni, D.-P.N.; Mirtaheri, M. Exploring the Effect of Near-Field Ground Motions on the Fragility Curves of Multi-Span Simply Supported Concrete Girder Bridges. *Infrastructures* **2024**, *9*, 19. https://doi.org/10.3390/infrastructures9020019

Academic Editor: Troyee Dutta

Received: 20 December 2023
Revised: 20 January 2024
Accepted: 22 January 2024
Published: 26 January 2024

1. Introduction

Highway bridges are important parts of infrastructure that link cities, towns, and villages, and act as the lifeline of transportation networks. They play a crucial role in facilitating the efficient and safe movement of people, products, and services across numerous locations, thereby supporting economic development. It has been recorded that certain bridges suffered damage during recent catastrophic earthquakes, including the 1971 San Fernando earthquake, the 1999 Chi-Chi earthquake in Taiwan, the 1995 Great Hanshin earthquake in Japan, and the 2010 Haiti earthquake [1–5]. Seismic vulnerability assessment plays a crucial role in identifying at-risk bridges and prioritizing retrofitting or replacement measures for unsafe bridges [6]. This is a valuable tool for evaluating the seismic vulnerability of bridges, and serves the aforementioned objectives.

The seismic vulnerability of a specific bridge or a class of bridges is evaluated using fragility curves [7]. A fragility curve depicts, at a specified level of ground motion intensity, the probability that a structure will experience a particular level of damage [8]. To put it another way, it illustrates the connection between the intensity of ground motion, like Peak Ground Acceleration (PGA), and the likelihood that a particular level of damage will occur to a structure. There are several methods that can be used to develop fragility curves for highway bridges, and each method has its own advantages and disadvantages. The expert opinion approach involves estimating the fragility of highway bridges using expert judgment [9]. The empirical approach is supported by a statistical study of damage data from previous earthquakes [10,11]. The analytical methods utilize mathematical models to predict the response of highway bridges to various hazard levels [12–16]. The hybrid method combines empirical and analytical methods to develop the fragility curves. The observed damage data are used in this method to assess and modify the model parameters to better match the observed damage data [17].

Even though the expert opinion and empirical methods are commonly used to develop fragility curves [18], there are limitations to these approaches. A limitation of the expert opinion method is its potential for bias or subjectivity. The fragility estimates are based on an individual's experience, knowledge, and perception of risk. Additionally, the expert opinion method may be limited by a lack of available data, particularly for hazards that occur infrequently or have not been studied extensively. The empirical method relies on observed damage data from past earthquakes. However, this method may be limited by the availability and quality of data. For example, damage data may not be available for all hazard intensities, or may not be representative of the current bridge inventory. Additionally, the empirical method may not account for changes in bridge design and construction practices over time. Both methods may also be limited by uncertainties in the input data and assumptions used in the analysis. Because of these limitations, additional techniques for creating fragility curves, such as the analytical method, are utilized, or other techniques are used to supplement the outcomes of these two techniques.

The analytical method for creating fragility curves is more widely used because it offers a more thorough understanding of the structural behavior of highway bridges under various levels of hazard, it can be used to simulate the impact of multiple hazards on the response of the bridge, and it permits consideration of uncertainties in the input data and assumptions used in the analysis. Analytical fragility calculation techniques are based on calculating the demand (D) at various intensity measures and the capacity (C) related to the defined damage levels. There are several techniques used in the demand calculation section, including spectrum analysis [19], nonlinear static analysis [20,21], and nonlinear dynamic analysis [22–25]. The demand and capacity are determined either for the overall bridge system or for the individual bridge components. System-level fragility curves take the entire bridge system into account as a single entity and calculate the likelihood that the bridge system will go beyond a particular damage state [26]. In contrast, component-level fragility curves consider the likelihood of particular bridge components, such as the deck, bearings, columns, or foundations, becoming damaged [26]. These curves can be used to assess the vulnerability of various bridge components to earthquakes and provide more thorough information regarding the performance of particular components [26].

It is possible to obtain the fragility curves for a particular bridge or a group of bridges. Fragility curves created for certain bridge classes can be used more broadly. The assessment of regional risk is one use of this class of fragility curve. An example of regional risk assessment is the loss assessment of roads, railways, and transportation networks. The development of these fragility curves requires long calculation times. Nielson and DesRoches [27] developed seismic vulnerability curves for nine categories of bridges (specifically, three-span and zero-skew bridges with non-integral abutments) commonly found in the central and southeastern regions of the United States. Fragility curves were created by Avşar et al. [28] for common highway bridges constructed in Turkey after the 1990s. Based on the skew angle, the number of columns per bent, and the number of spans, four major bridge classes were used. On the other hand, fragility curves created for a particular bridge have limited applications, and may be used for seismic evaluation or risk assessment of that bridge. Tavares et al. [29] developed a fragility curve for the Chemin des Dalles Bridge located in Quebec, Canada. Mackie and Stojadinovic [30] compared three methods for obtaining the probabilistic seismic demand models (PSDM): cloud, incremental dynamic, and stripe. Mangalathu and Jeon [31] presented a framework for generating bridge-specific fragility curves by leveraging machine learning and a strip-based approach. Kiani et al. [32] explored the application of machine learning tools for predicting structural responses and fragility curves. They investigated ten classification-based methods, generating structural responses through multiple strip analyses. It was observed that quadratic discriminant analysis and random forest were preferred for both balanced and imbalanced datasets due to their superior efficiency in predicting structural responses.

The component-level fragility curves produced using nonlinear dynamic analysis are more precise than those produced using other techniques. Strong ground motions in the form of time history are the inputs in the nonlinear dynamic analysis of structures. Strong ground motion characteristics have a significant impact on the outcomes of nonlinear time history analysis, and this impact can change the produced fragility curves. Strong ground motions are split into far-field and near-field ground motions as a result of this distinction. Twenty kilometers can be regarded as the threshold distance for differentiating between near-field and far-field ground motions [33]. Although Mansouri et al. [34] showed that in areas far away from faults, it is very important to consider the duration and intensity of earthquake records, and that these earthquakes can have a destructive effect on structures, in contrast to far-field ground motions, near-field ground motions are characterized by strong velocity and long-period displacement pulses, have destructive potential, and may have more severe effects [35]. Earthquakes in Northridge (1994), Kobe (1995), and Chi-Chi (1999) are examples of near-fault events. Compared to far-field earthquakes, "forward-directivity" sites experience a concentrated release of seismic energy within a short duration, resulting in significantly increased demands on engineering structures [36,37]. A common characteristic of near-fault ground motion, known as the "fling step", is recognized by a singular high-amplitude velocity pulse accompanied by a lasting ground offset. This phenomenon occurs parallel to either dip or strike directions [38]. The two types of near-field ground motions, forward-directivity and fling step, have pulses that are one-sided for the fling step and two-sided for the forward directivity. This means that the fling step motion causes permanent displacement of the ground, whereas the forward directivity motion does not.

Given the importance of researching the impact of near-fault records on fragility curves, not many studies have been conducted in this area. Baig et al. [39] conducted a fragility analysis on a continuous steel box-girder bridge, taking into account the impacts of both far-field and near-field earthquakes. They demonstrated that the fling step and the impact of near-field directivity pulses represent a significant risk to the bridge, even at modest PGA values. Mosleh et al. [40] assessed the seismic vulnerability of typical bridges constructed prior to 1990, subjecting them to both near-fault and far-field strong motions. While their focus was on bridge columns, they suggested that future investigations should encompass bearings and abutments as well. Billah et al. [41] concentrated on evaluating the seismic vulnerability of retrofitted multi-column bridge bents, examining their response to both far-field and near-fault ground motions. Although comparing the four retrofitting techniques is the major goal of this study, a comparison of the impact of near and far-field records on fragility curves was also explored. They reported that, owing to the impulsive effect of near-fault loading, near-fault ground motions increased the vulnerability of retrofitted bridge bents. Naseri et al. [42] examined the impact of near-fault and far-field ground motions on the seismic behavior of horizontally curved multi-frame RC box-girder bridges, taking into account the vertical component of the earthquake ground motions. The conclusions show that the seismic vulnerability of this bridge subclass is reasonably increased by the near-field effects. Chen [43] conducted a study on the seismic performance of tall-pier bridges when exposed to ground motions originating from near-fault sources. The investigation employed probability-based fragility analysis to assess the behavior of the entire bridge system. This type of bridge is typical in Southwest China. Peak Ground Velocity (PGV) was utilized as an intensity metric in the aforementioned study, and the effects of near-field and far-field ground motions were not compared. Shao et al. [44] conducted an analysis on the influence of vertical components of near-field ground motions on the fragility surface of bridges. Fragility surfaces share similarities with fragility curves; however, a notable distinction exists. While fragility curves offer the probabilities of encountering particular types of damage based on a single intensity parameter of ground motions, fragility surfaces present this probability by considering two intensity parameters.

The number of studies on the effect of near-fault ground motions on bridge fragility curves is slight. Several studies simply employed near-field records without comparing them to far-field ones. Numerous types of bridges exist, some of which are not covered [45,46]. In addition, the types of fragility curves created, whether for the entire system or for individual components, vary. Further study in this area is essential due to the research's limitations. In this study, for the first time, the effects of near-field earthquakes on the fragility curves of the constituent components of simple multi-span concrete bridges are investigated in detail. In this investigation, ground motions containing strong velocity pulses, and ground motions without these pulses, are applied to the bridge structure, and the results and responses are recorded and compared. A comparison of the fragility curves of the ground motions with and without pulses will lead to interesting results.

Multi-Span Simply Supported Concrete (MSSS Concrete) girder bridges are the type of bridges being studied. Over 20% of bridges in the Central and Southeastern United States (CSUS) are of this type, which is a common form. The key aspect to consider here is that research on a particular bridge is necessary due to the substantial number of these bridges on the highways. By concentrating on a specific structure, the level of uncertainty is decreased, and the influence of a particular uncertainty, such as the distance from the fault, can be assessed more precisely. Therefore, it is important to investigate the seismic vulnerability of these, as well as the effect of ground motion types on their fragility curves. Records from the far-field and near-field are selected in two categories. Using these two kinds of records for the column curvature, abutment displacement, expansion bearing, and fixed bearing as bridge components, fragility curves for the bridge are produced. The fragility curves of the bridge's individual components are compared for both near-field and far-field ground motions, and the impact of various ground motion types is examined.

2. Development of Analytical Fragility Curve

Fragility curves represent conditional probabilistic assessments that indicate the likelihood of a structure experiencing or surpassing a designated level of damage corresponding to a specific ground motion intensity (*IM*). In other words, under a specific intensity measure, the fragility curve calculates the probability that the seismic demand (*D*) will exceed the bridge capacity (*C*). The fragility curve is a conditional probability, expressed as P[$D > C \mid IM$]. This probability distribution is usually modeled as a log-normal distribution. The log-normal model is used because the outcomes of this probabilistic model are in strong agreement with the actual data. It has also been demonstrated that this conditional probability will have a log-normal distribution if capacity and demand both have log-normal distributions [47]. Therefore, the fragility curve can be represented as a cumulative log-normal distribution function, as expressed by the following formula:

$$P[\, D > C|IM \,] = \Phi\left[\frac{\ln\left(\frac{S_d}{S_c}\right)}{\sqrt{\beta_{D|IM}^2 + \beta_C^2}}\right] \tag{1}$$

where *Sd* denotes the median estimate of the demand derived from the intensity measure *IM*, *Sc* represents the median estimate of the capacity, $\beta_{D|IM}$ indicates the logarithmic standard deviation of the demand given the intensity measure, βc represents the capacity dispersion, and Φ is the standard normal cumulative distribution function; thus, once the four parameters, namely Sd, Sc, $\beta_{D|IM}$, and βc, have been estimated, it becomes feasible to determine the fragility of any individual bridge component. A Bayesian approach that integrates both physics-oriented evaluations and judgmental-based assessments is employed to develop log-normal parameters (Sc, βc) for the limit states of each bridge component [48].

To develop fragility curves (see Figure 1), Probabilistic Seismic Demand Models (PSDM) are required. These models create a connection between Engineering Demand Parameters (*EDP*) and Intensity Measures (*IM*), usually formulated using linear regression methods. There are various approaches to establish a relationship between *IM* and *EDP*. Some methods utilize unscaled ground motions, whereas others utilize scaled ground motions. In the latter case, ground motions are scaled in a specific manner to achieve the desired *IM*. One such technique is known as Incremental Dynamic Analysis (IDA). On the other hand, the Cloud method employs unscaled records [14,24]. For this study, the Cloud method is utilized.

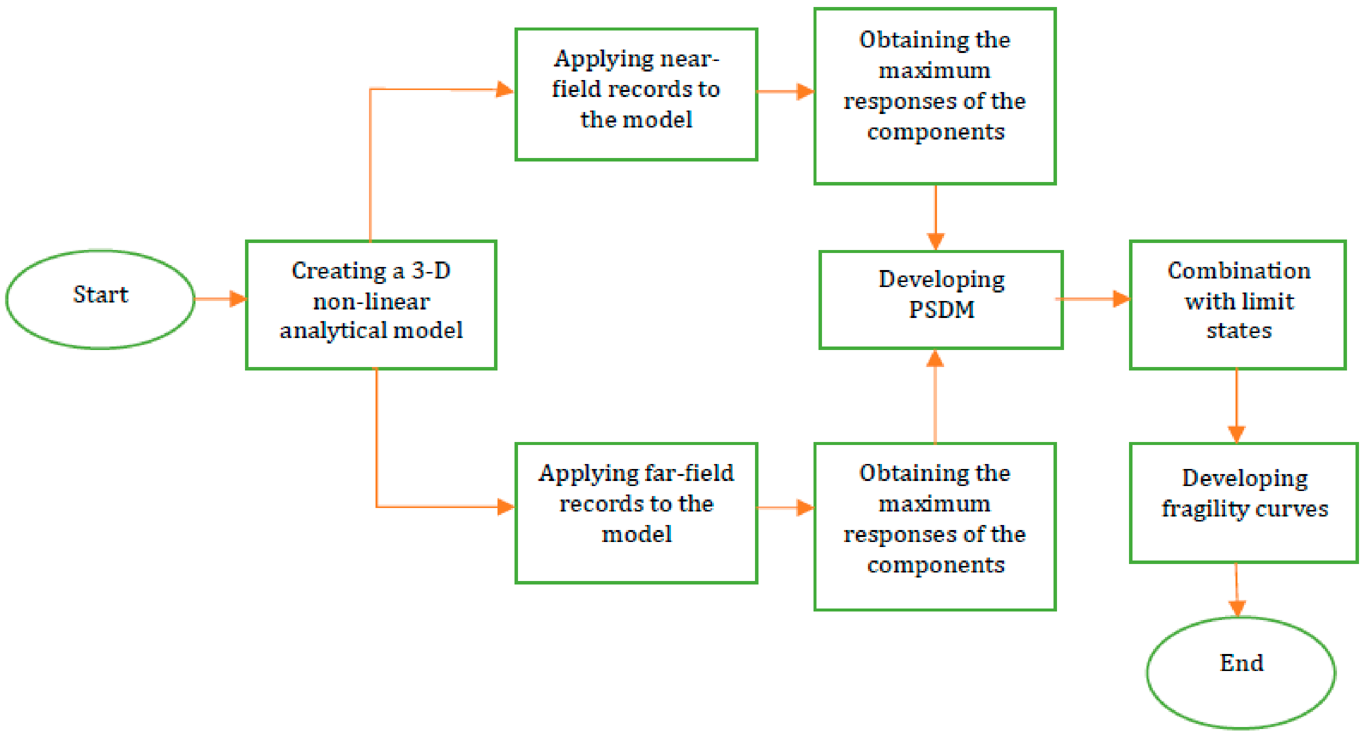

Figure 1. Creating fragility curves.

Cornell et al. [49] proposed that the median demand estimate (Sd) can be represented using a power model. This association is defined by Equation (2), with 'a' and 'b' serving as the regression parameters.

$$S_d = a(IM)^b \tag{2}$$

The logarithm operator is used on both sides of the above equation to convert the non-linear relationship into a linear one. The parameters of this relationship are obtained using linear regression. In the regression analysis, the maximum response from the nonlinear dynamic analysis (d_i) is utilized as the output model, and the *IM* of each corresponding input record is used as the input model. The regression analysis is applied independently to both far-field and near-field ground motions. The estimation of the dispersion of demand conditioned on the *IM* can also be derived through regression analysis using the following equation:

$$\beta_{D|IM} \cong \sqrt{\frac{\sum_{i=1}^{N}\left(\ln(d_i) - \ln\left(a\ IM^b\right)\right)^2}{N-2}} \quad (3)$$

where N is the total data, which is the number of nonlinear dynamic analyses performed. It is important to note that N for a near-field dataset can vary from that for a far-field dataset.

3. Bridge Modeling and Configuration

The reference model for this study is an MSSS concrete girder bridge, previously examined by Nielson [50]. The assessment of the bridge model under investigation is depicted in Figure 2. The bridge under consideration has a total length of 48.8 m, with two side spans measuring 12.2 m each and a middle span spanning 24.4 m. It is composed of four expansion joints, with two located at the top of the bents and the remaining two positioned at the abutments. The width of each span is 15.01 m, and the bridge is built with prestressed girders [50].

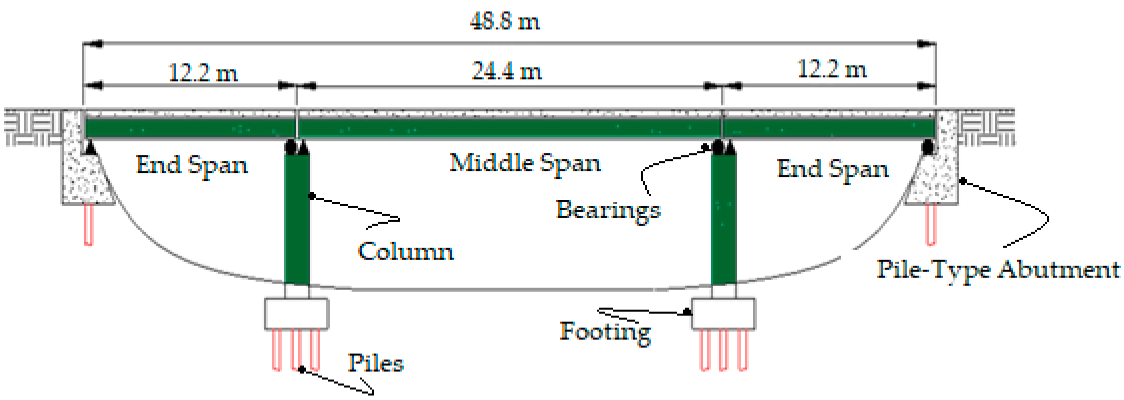

Figure 2. Under study bridge model elevation.

The bridge's end spans receive support from a pile-type abutment at one end and a multi-column bent at the opposite end. As for the middle span, it is supported by two multi-column bents at its ends. Each multi-column bent consists of a reinforced concrete bent beam that measures 1066.8 mm in width and 1219.2 mm in depth. This bent beam is supported by three circular reinforced concrete columns, each with a diameter of 914 mm and a height of 4600 mm. In terms of reinforcement, the bent beam utilizes 15-#29 and 4-#16 reinforcing bars distributed across its cross-section. The transverse steel reinforcement consists of #16 stirrups spaced at an average interval of 305 mm, as illustrated in Figure 3 [50]. In contrast, the columns employ 12-#29 bars for reinforcing along their length, with #13 transverse bars spaced at 305 mm to confine them, as illustrated in Figure 3. The concrete utilized in the construction has been designed to possess a strength of 20.7 MPa. The yield strength of the reinforcing steel is 414 MPa. The specifications for these column details were obtained from a study conducted by Hwang et al. [51].

The bridge is equipped with elastomeric pad bearings, and the performance of fixed bearings and expansion bearings are different under the influence of earthquake force. Their deformations against near-field and far-field earthquakes are studied in this research. The bearings incorporate two steel dowels measuring 25.4 mm in diameter, as illustrated in Figure 4. The elastomeric pads for the middle span have dimensions of 406 mm in length, 152 mm in width, and a thickness of 25.4 mm. On the other hand, the pads for the side spans are slightly larger, measuring 559 mm in length, 203 mm in width, and also 25.4 mm in thickness. The primary distinction between fixed-type and expansion-type bearings lies in the dimensions and configurations of the holes intended for the steel dowels. These fixed and expansion bearings are positioned alternately throughout the bridge's length, represented by triangles and circles in Figure 2 [50].

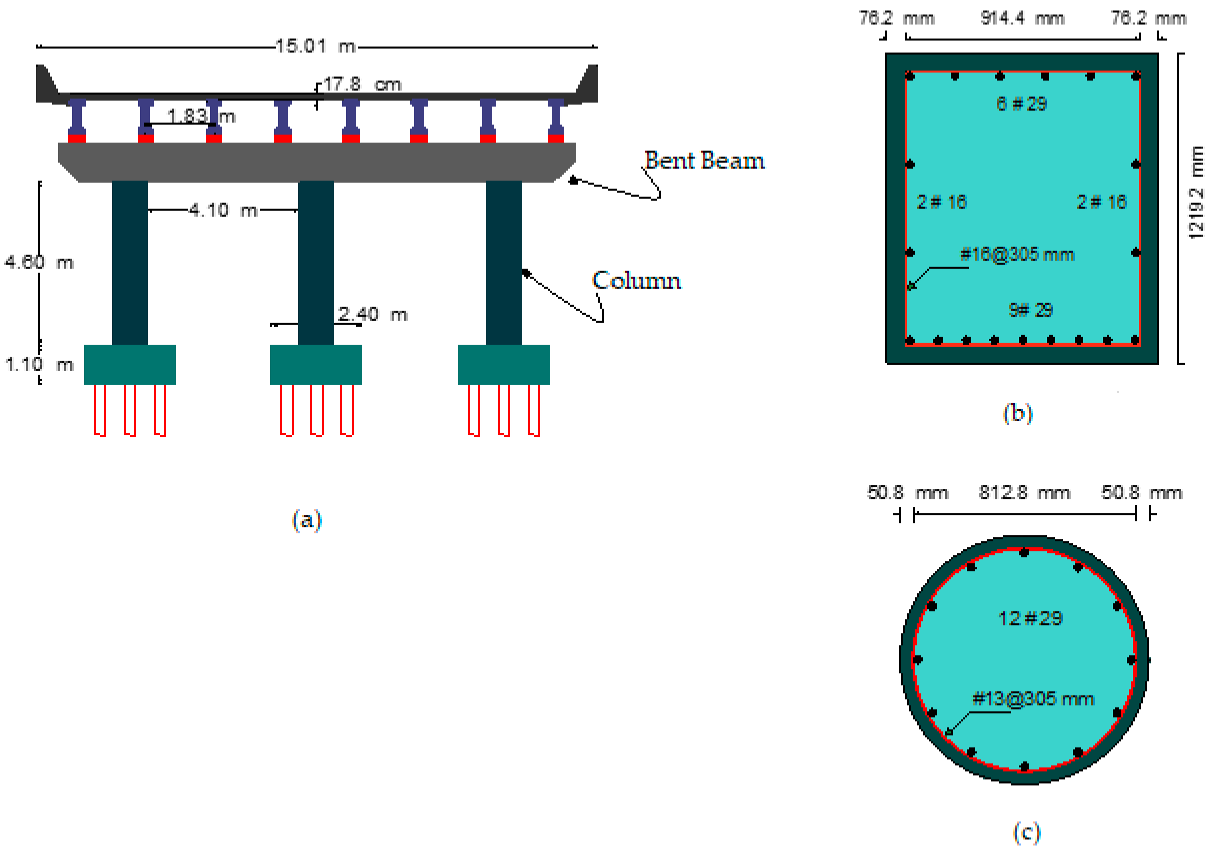

Figure 3. Bridge configuration: (**a**) pier and deck, (**b**) bent beam section, (**c**) column section.

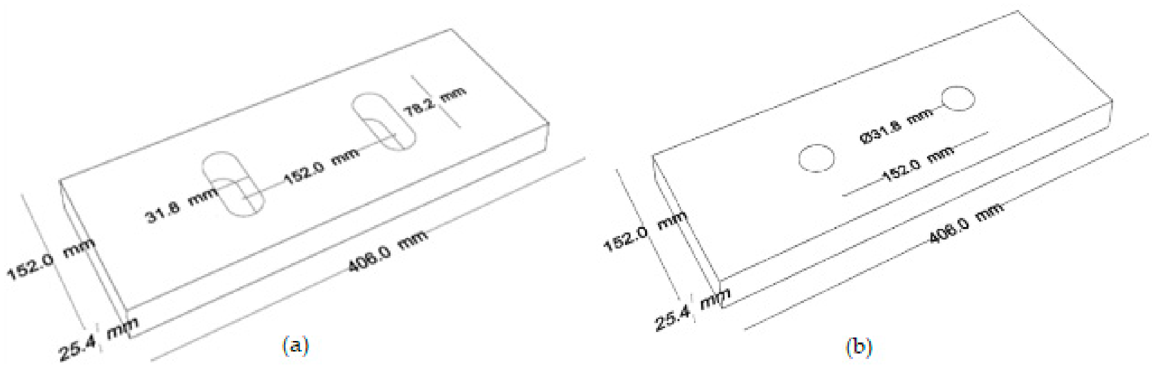

Figure 4. Elastomeric bearings used for bridge girders: (**a**) expansion bearing, and (**b**) fixed bearing.

The pile caps utilized in this design are reinforced concrete footings measuring 2438 mm square and 1092 mm in thickness. The reinforcement is placed on the bottom side of the pile caps. The layout involves eight piles that are embedded approximately 305 mm into the bottom of the footing, without any positive connection provided between them. The connection between the pile cap and the columns is established through lap splices that are 914 mm in length and located at the bases of the columns.

Utilizing the OpenSees analysis platform [52], a comprehensive non-linear 3D model has been developed for the bridge under investigation. The behavior of the composite girder and slab section is presumed to be linear, and they are represented through the use of elastic-beam column elements in the model. To address the issue of pounding between the decks, the model utilizes the contact element approach. This approach is based on the research conducted by Muthukumar and DesRoches [53], where they comprehensively described and incorporated the phenomenon of pounding and its associated energy dissipation in the model. However, to acknowledge the variability of damping in the structural response, it is treated as a random variable. This means that the model considers the inherent variability of damping and its potential influence on the dynamic behavior of the structure.

The model utilizes non-linear beam-column elements to represent the columns. Each element is characterized by fibers that exhibit distinct stress–strain relationships corresponding to the specific material properties. The materials employed include unconfined concrete, confined concrete, and longitudinal reinforcing steel. Similarly, the simulation of bent beams in the model utilizes identical elements as those applied to the columns. To streamline the analysis, rectangular cross-sections are assumed for the bent beams.

The model includes the integration of bearings using non-linear translational springs, which collectively consider the effects of elastomeric pads and steel dowels. Elastomeric pads are represented with an perfectly elastic plastic material, and their initial stiffness is determined by the geometric properties of the pads. Non-linear translational springs are employed to accurately simulate the behavior of the abutments. The stiffness of these springs is influenced by both the stiffness of the piles and the passive resistance of the soil. The recommended approach provided by Caltrans [54] is followed to calculate the spring constants. Similarly, for the rotational and translational springs associated with the pile foundations, the same approach is employed. This method incorporates relevant parameters and characteristics to determine the appropriate constants.

4. Selecting Ground Motion Time-Histories

The aim of this section is to choose a set of far-field and near-field ground motions that will be used to produce fragility curves in the following sections. Baker's [55] work was used to choose near-field records. These are a total of 91 records of different earthquakes (Kobe, Japan, Chi-Chi, Taiwan, North Ridge, Imperial Valley, and Loma Prieta) were obtained. In Baker's study, the goal was to identify records that exhibit a large pulse in the velocity time history due to the forward directivity of near-fault records. The extracted pulse magnitudes were compared to the original ground motion as a criterion for categorizing a ground motion as having pulse-like characteristics. The obtained pulses were extracted using the Wavelet transform [56]. A sample of records was used to train a classification algorithm, which was then used to 3500 data from the Next Generation Attenuation (NGA) project to select 91 records. All records can be accessed on the website http://peer.berkeley.edu/nga (accessed on 25 August 2020). All pulse-like records have a magnitude greater than 5.5, and have been recorded at a distance of 30 km [55]. The maximum acceleration of these earthquakes (PGA) ranges from 0.09 g to 1.43 g. The acceleration history of a near-field record example is depicted in Figure 5. The figure illustrates a distinct pulse present in the acceleration history of this particular record. Notably, the pulse becomes even more pronounced when examining the speed history.

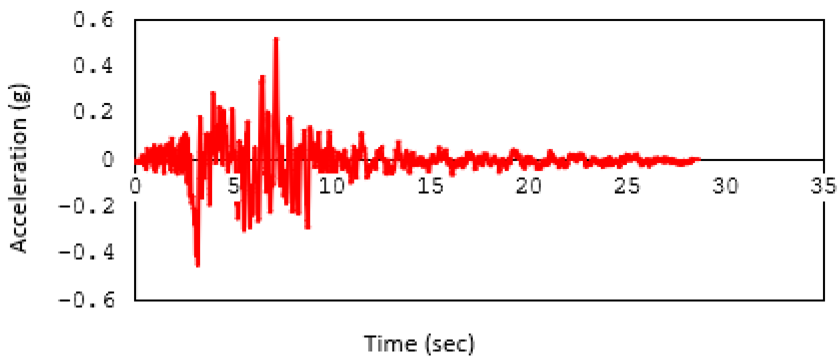

Figure 5. An example of a near-field record acceleration time history.

The work of Haselton and Deierlein [57] is referenced for the selection of far-field records in the model. Their research primarily focused on evaluating the seismic collapse safety of reinforced concrete moment frame structures constructed in compliance with the International Building Code. They introduced a methodology for evaluating structural collapse. They chose a number of general far-field records for their study. Their method of selection differs from site-specific record selection, which is applicable only to a single site. To address the aforementioned concerns, this study employs the records selected by Haselton and Deierlein [57]. The selected records adhere to the following specifications:

- Magnitude exceeding 6.5.
- Source-to-site distance exceeding 10 km (calculated as an average of Campbell and Joyner–Boore distances).
- Exceeding 0.2 g in peak ground acceleration and surpassing 15 cm/s in peak ground velocity.
- The shear wave velocity of soil in the top 30 m exceeding 180 m/s, determined by NEHRP soil types A-D (It is important to mention that all chosen records coincidentally occurred on C/D sites).
- A limitation is placed on the inclusion of records to a maximum of six from a singular seismic event. When the initial criteria are met by more than six records, the selection is determined by the six records with the highest peak ground velocity (PGV). However, in certain instances, a record with a lower PGV may be considered if the peak ground acceleration (PGA) is notably higher.
- The lowest usable frequency is set below 0.25 Hz to ensure that the low-frequency content is not filtered out during the filtering process.
- The records correspond to seismic activity along strike-slip and thrust faults, and align with seismic events in California.
- Spectral shape (ε) is not taken into account.
- Station housing is not taken into account, but the selected PEER-NGA records are considered "free-field" records.

Figure 6 displays the acceleration spectra of the selected records. It shows the acceleration spectra of both the near-field and far-field records, as well as the median of the spectra. All records have been scaled to a PGA of 0.4 g to facilitate the comparison of spectra and dispersion. This scaling ensures that the intensities of all the records are uniform. Additionally, the figure includes a comparative analysis of the near-field and far-field records. Notably, it is evident that the spectra of near-field records exceed that of far-field records in longer periods. According to the NEHRP classification, earthquake records in the far-field indicate that the soil conditions are predominantly C or D, which suggests that the soil quality is average. On the other hand, the soil type is not specified in the near-field records, which means that all NEHRP classification groups may be represented. As a result, it can be inferred that the soil conditions in both the near-field and the far-field are generally average, and no separate comparison has been made here regarding the impact of local soil conditions.

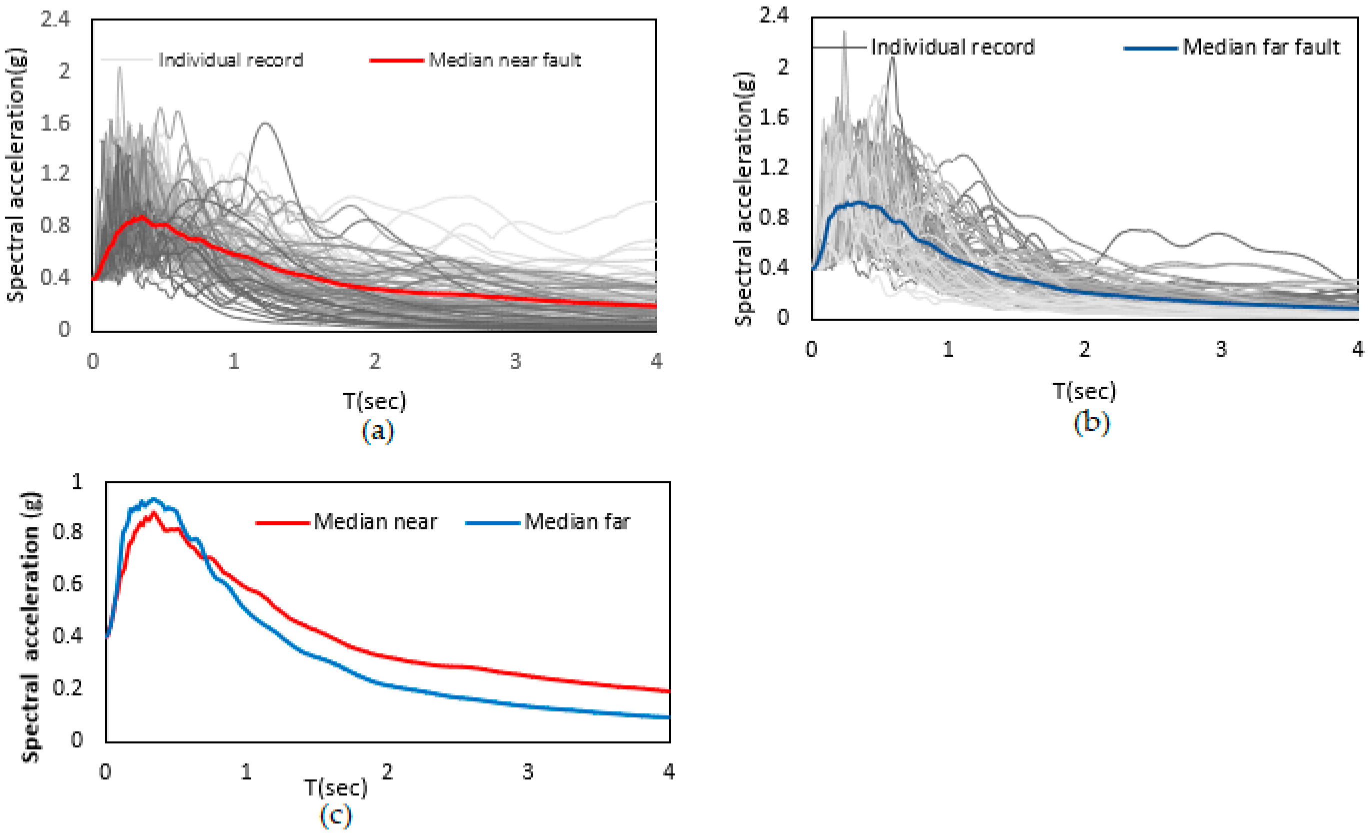

Figure 6. Acceleration spectrum of selected records: (**a**) near-field records, (**b**) far-field records, and (**c**) a median comparison between near-field and far-field records.

5. Limit States

One of the important steps in generating fragility curves is to determine the limit states for various components of the bridge. The limit states in this study were obtained from the limit states defined by FEMA in the damage assessment package HAZUS [58,59]. These damage states include slight, moderate, extensive, and complete collapse. To generate the fragility curves associated with each damage state, the response values of the bridge components that cause these damage states must be determined. For example, the ductility value of a column should be determined in the specified damage states This means that the minimum values of ductility that cause column damages in four states, including slight, moderate, extensive, and complete collapse, should be determined. The response values associated with the damage states are called limit state capacities. In this study, the limit state capacities were obtained from the work of Nielson and DesRoches [27]. As the damage state capacities have a log-normal probability distribution, both the median and dispersion values must be determined. Table 1 shows the values of the concrete column ductility, Elastomeric Bearing Fixed joint (mm), Elastomeric Bearing Expansion joint (mm), abutment–passive (mm), and abutment–active (mm) for the four damage states [27]. As can be observed, the dispersion and median values of damage state capacities are presented in this table.

Table 1. Capacity limit estimates for as-built components (adapted from Nielson and DesRoches [27]).

Component	Slight		Moderate		Extensive		Complete	
	Med	**Disp**	**Med**	**Disp**	**Med**	**Disp**	**Med**	**Disp**
Concrete Column (μc)	1.29	0.59	2.1	0.51	3.52	0.64	5.24	0.64
Elastomeric Bearing Fixed-Long (mm)	28.9	0.60	104.2	0.55	136.1	0.59	186.6	0.65
Elastomeric Bearing Expan.-Long (mm)	28.9	0.60	104.2	0.55	136.1	0.59	186.6	0.65
Abutment-Passive (mm)	37	0.46	146	0.46	N/A	N/A	N/A	N/A
Abutment-Active (mm)	9.8	0.7	37.9	0.9	77.2	0.85	N/A	N/A

6. Probabilistic Seismic Demand Models

This section provides a description of the process involved in developing probabilistic seismic demand models (PSDM). For all chosen near-field and far-field records, nonlinear time history analysis is carried out, and the response of every bridge component is recorded. The bridge components considered in this study are columns, fixed bearings, expansion bearings, and abutments. The component demands are subsequently graphed in relation to the PGA of the ground motions. A summary of the method performed is provided below.

Once a three-dimensional analytical model is constructed, it is subjected to 91 near-field records and 78 far-field records in the longitudinal direction for analysis. The Ground Motion Selection section contains a detailed explanation of how to choose near-field and far-field records. The important components of the bridge structure that were recorded in each implementation of the program to create a fragility curve are as follows:

1. Longitudinal displacement of the abutment in a passive situation or in a state where it moves towards the soil behind.
2. Longitudinal displacement of the abutment in the active state or in a state where it moves away from the soil behind.
3. Bearing deformations in fixed supports in the longitudinal direction.
4. Bearing deformations in free supports in the longitudinal direction.
5. Maximum curvature in the columns.

The logarithm of the maximum response value of each component is plotted against the logarithm of the intensity measure after completing nonlinear dynamic analysis and recording the maximum response under each record. The model coefficients a and b are calculated by performing linear regression between $\ln(d_i)$ and ln (PGA) in order to produce a probabilistic seismic demand model. It should be emphasized again that the regression procedure is carried out independently for near-fault and far-field records in order to calculate the coefficients a and b. Figure 7 shows the PSDM diagrams related to the displacement of the abutment in the passive state, i.e., when the abutment moves towards the back soil, and also in the active state, i.e., when the abutment undergoes displacement away from the surrounding soil. These diagrams are plotted for both the near-field earthquakes and the far-field earthquakes. This figure also provides the related PSDM equations. It is clear that the PSDMs for near-field and far-field data differ.

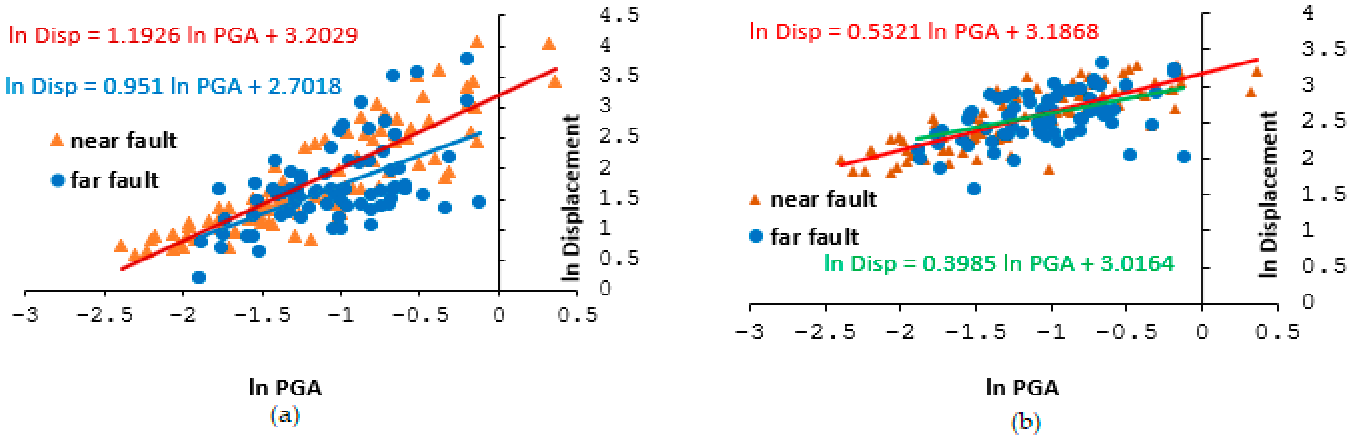

Figure 7. Probabilistic seismic demand models for abutment displacement: (**a**) passive state, and (**b**) active state.

7. Results

In this section, the component fragility curves for the studied multi-span simply supported (MSSS) concrete girder bridge are generated. For this purpose, the probabilistic seismic demand model presented in the previous section and the limit state damage capacities are combined. Equation (1) is used to create fragility curves. Because the probabilistic seismic demand model was separately produced for near-field and far-field records, two types of fragility curves are produced. Fragility curves are generated for five bridge components and four damage states for the far-field and near-field records. The fragility curves for the far- and near-field records are compared with one another. The mentioned comparison is the main purpose of this article. Figure 8 shows the fragility curves of abutment displacement in the passive state. Fragility curves are presented for the far-filed and near-fault records. As is evident from the observations, this bridge is more vulnerable under near-field records. The probability of exceeding the slight damage state is higher under the near-field records than under the far-field records. It can be seen that at PGA equal to 1 g, the probability of exceeding the slight state is more than 30%, which shows the susceptibility of the bridge under near-field records. The discrepancy between the fragility curves of near-field and far-field records increases as PGA rises. Fragility curves for extensive and complete collapse are absent from the presentation, as Nielson and DesRoches [27] do not provide the corresponding capacity values for these limit states. Therefore, it is impossible to include fragility curves for extensive and complete collapse in the analysis.

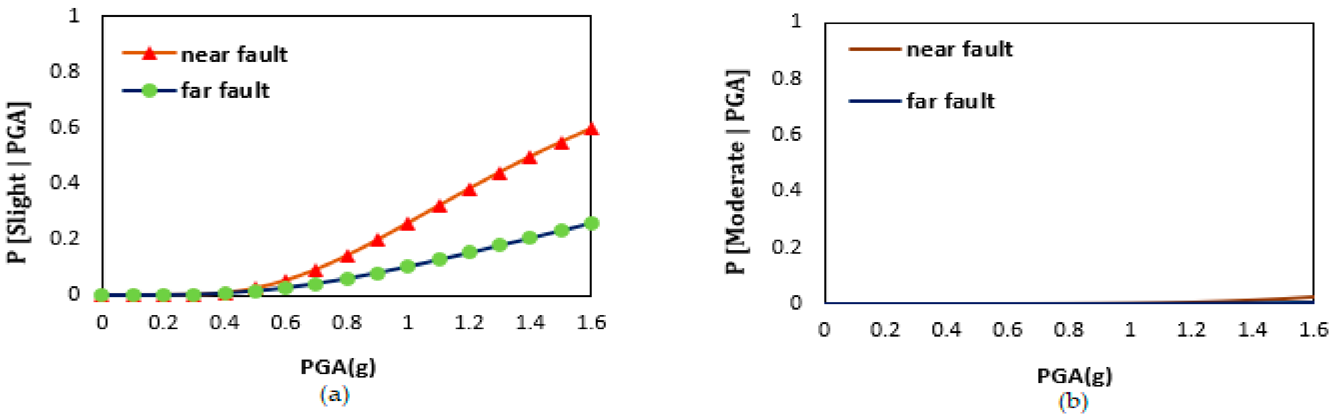

Figure 8. Fragility curves of abutment displacement in passive state: (**a**) slight damage state, and (**b**) moderate damage state.

The abutment displacement fragility curves under the active conditions are demonstrated in Figure 9. Fragility curves are provided for both the near- and far-field records. The fragility curves for the complete collapse state are not presented because of the unavailability of capacity values corresponding to this particular limit state in Nielson and DesRoches [27]. However, fragility curves are provided for the remaining limit states, namely slight, moderate, and extensive collapse.

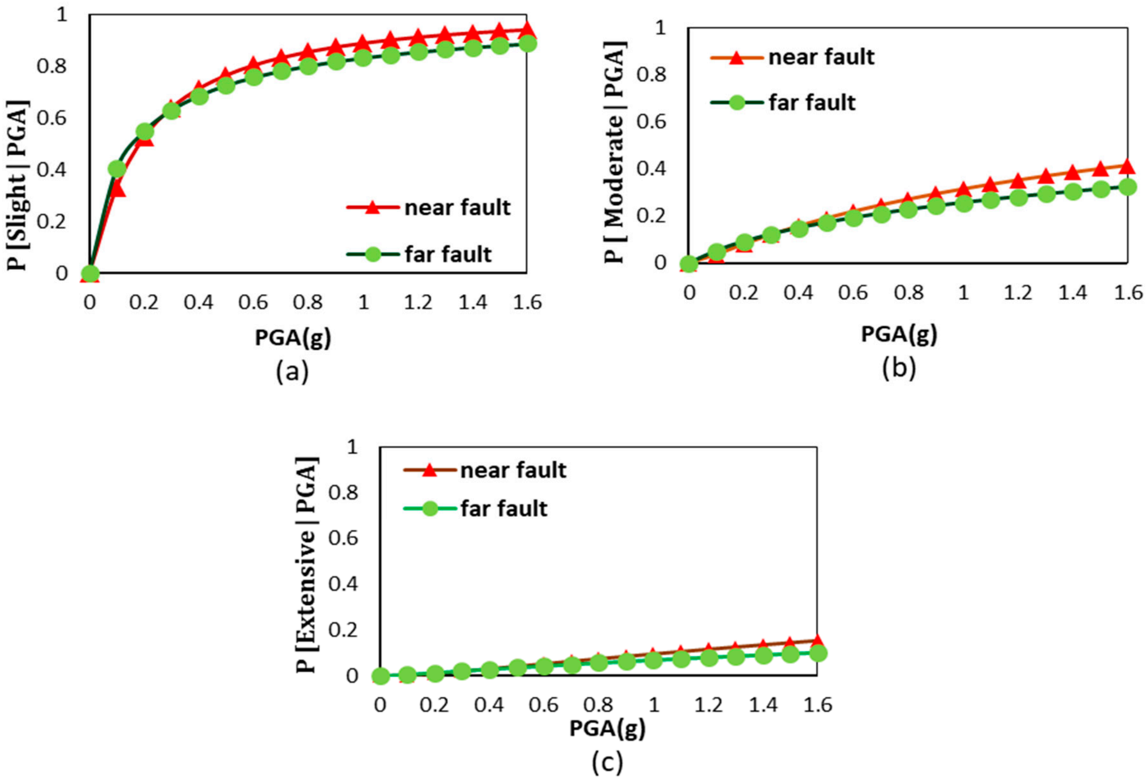

Figure 9. Fragility curves of abutment displacement in the active state: (**a**) slight damage state, (**b**) moderate damage state, and (**c**) extensive damage state.

The difference between the near-field and far-field curves shows patterns that are comparable to the abutment displacement in the passive state. Nonetheless, the probability of surpassing the damage states is decreased compared to the abutment displacement in the passive state, indicating that the bridge is less vulnerable in this state.

The fragility curves for column curvature are shown in Figure 10. Fragility curves are presented for four different limit states: slight, moderate, extensive, and complete collapse. The results of both the near-field and far-field records are displayed. As can be observed, there is no discernible difference between the near- and far-field records at low intensities. Nevertheless, at high intensities, the bridge is more vulnerable to near-field records.

The fixed bearing deformation's fragility curves are shown in Figure 11. For each limit state, two graphs are provided: one for near-field records and another for far-field records. In this scenario, the fragility curves for four different limit states—slight, moderate, extensive, and complete collapse—are illustrated. In contrast to the above cases, where the bridge is consistently more vulnerable under near-field records, these fragility curves show an inconsistent pattern. The impact of far-field records is more significant at low intensities, whereas that of near-field records is more pronounced at high levels. In this conclusion, 0.8 g roughly marks the transition between high and low intensity.

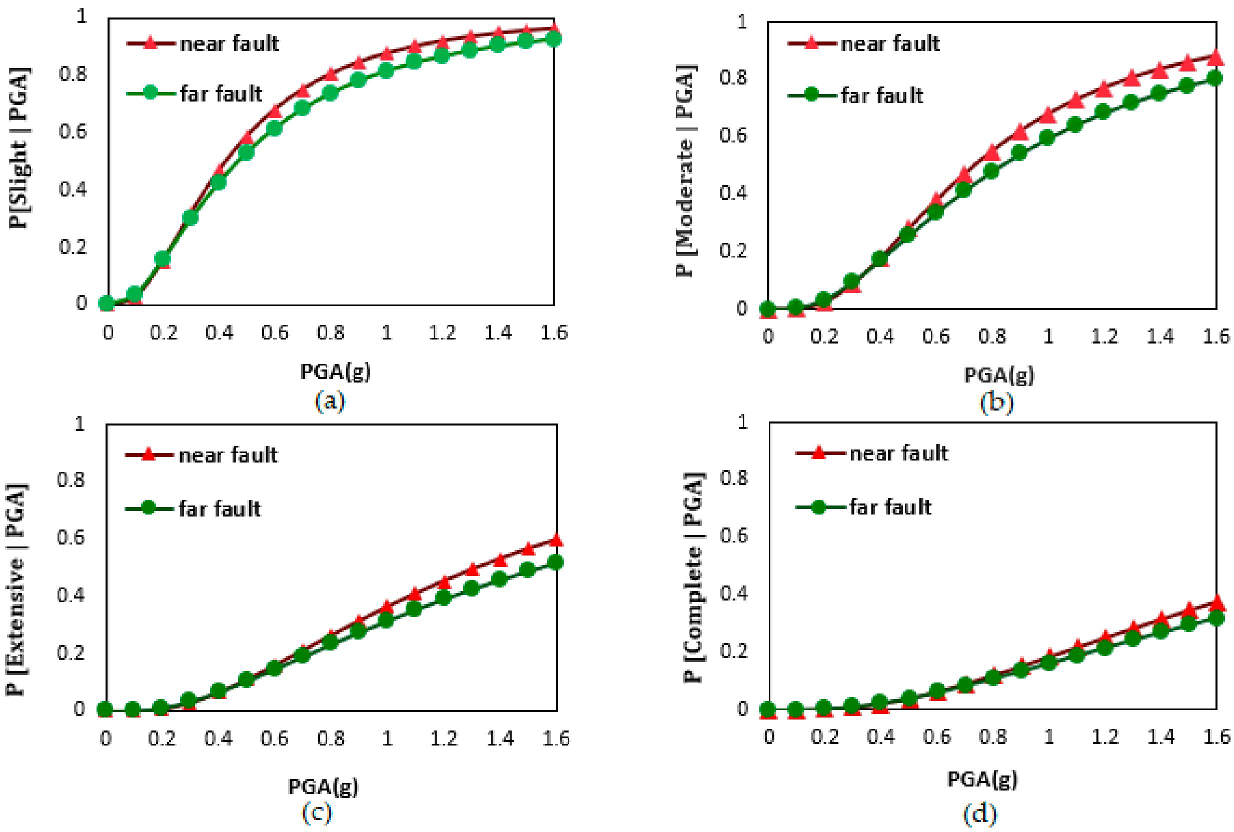

Figure 10. Fragility curves of column curvature: (**a**) slight damage state, (**b**) moderate damage state, (**c**) extensive damage state, and (**d**) complete collapse damage state.

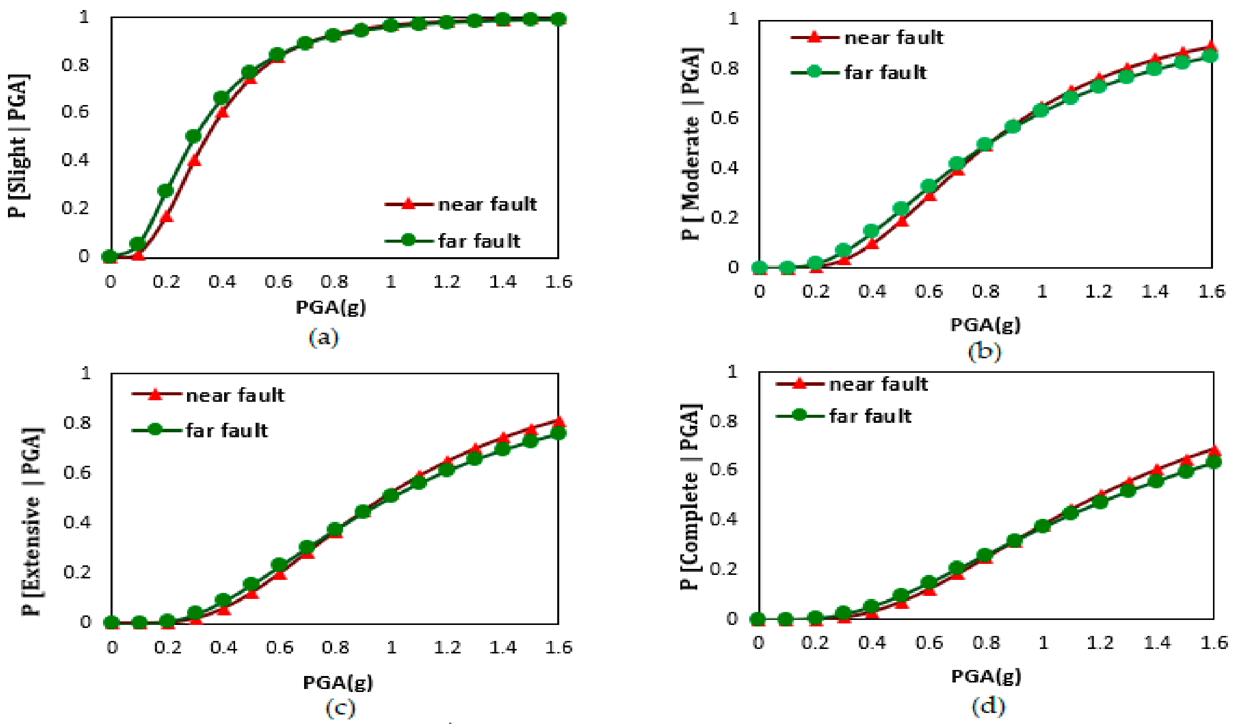

Figure 11. Fragility curves of fixed bearings deformation: (**a**) slight damage state, (**b**) moderate damage state, (**c**) extensive damage state, and (**d**) complete collapse damage state.

The fragility curves of the expansion-bearing deformation are shown in Figure 12. Fragility curves were illustrated for both far-field and near-field records. Fragility curves are presented for four distinct limit states: slight, moderate, extensive, and complete collapse. The differences between near-field and far-field ground motion records are negligible at very low intensities. The bridge is more vulnerable under near-field records at high intensities.

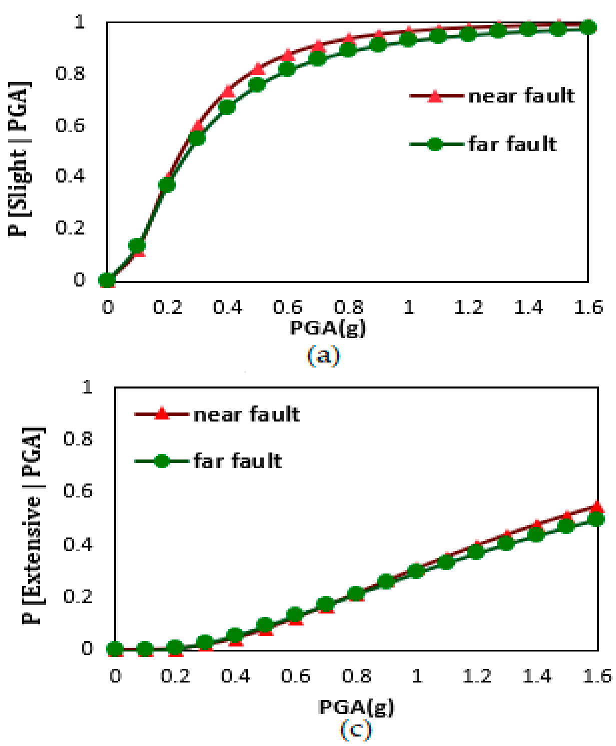

Figure 12. Fragility curves of expansion bearings deformation: (**a**) slight damage state, (**b**) moderate damage state, (**c**) extensive damage state, and (**d**) complete collapse damage state.

8. Conclusions

In this study, the effect of near-field ground motions on fragility curves is investigated. The investigation focuses on multi-span simply supported concrete girder bridges, which are widespread throughout the Central and Southeast of the US. Two ground motion sets from the far-field and the near-field ground motions are selected. Component fragility curves are produced for three key parameters: column curvature, abutment displacement, and bearing deformation. The fragility curves based on near-field records and their counterparts based on far-field records are then compared. These are the findings of the investigations:

1. Comparing the fragility curve of the near-fault earthquake in the case of abutments and columns with the fragility curve of the far-field shows that in all limit states, including slight, moderate, extensive, and complete, and in all intensities related to PGA, the near-fault earthquake damage is more severe than the far-field earthquake damage. As the PGA increases, the difference in damage between near-fault and far-field earthquakes increases.
2. The greatest impact of the near-fault earthquake is on the fragility curve of the abutment in the passive state, which in high-intensity earthquakes in the slight damage state, the difference with the effect of the far-field earthquake is about 33%.
3. In the case of bearings, the impact of near-fault earthquakes on bearings deformation in earthquakes with a lower PGA (about 0.8 g) is less than that of far-field earthquakes. The available evidence suggests that fragility curves pertaining to the far-field exhibit

a more critical state. In the case of earthquakes with higher PGA, the damage of the near-fault earthquake is greater than that of the far-field earthquakes.

4. In all components except for fixed bearings, as the graphs show, in low PGAs, i.e., up to 0.4 g, the effects of earthquakes in the near- and far-fields do not differ much.
5. Compared to expansion bearings, fixed bearings are significantly more vulnerable to near-field and far-field earthquakes in all limit states; this is more evident in higher PGAs.
6. As the figures show, the weakest component against near-field and far-field earthquakes in all limit states are fixed bearings.

9. Limitations and Future Research Needs

This research was conducted on concrete bridges with multi-span simple supports. In the future, similar studies can be carried out on bridges with different specifications to investigate their vulnerability to earthquakes in the fields near the fault. It would be a good idea to compare the vulnerability of bridges with different geometries and materials against the impact of earthquakes in the near field. In this research, the peak ground acceleration (PGA) has been used as a measure of earthquake intensity. For future research, using advances in machine learning [31,32,45,60–64] can enable the extraction of effective earthquake features and the creation of PSDM curves based on these features.

Author Contributions: Conceptualization, H.S. and M.M.M.; methodology, H.S., M.M. (Mohammadreza Mashayekhi), M.M.M. and D.-P.N.K.; software, H.S. and D.-P.N.K.; validation, M.M. (Mohammadreza Mashayekhi), M.M.M. and D.-P.N.K.; formal analysis, H.S. and D.-P.N.K.; investigation, H.S. and D.-P.N.K.; resources, M.M. (Mohammadreza Mashayekhi), M.M.M., D.-P.N.K. and M.M. (Masoud Mirtaheri); data curation, H.S., M.M. (Mohammadreza Mashayekhi) and D.-P.N.K.; writing—original draft preparation, H.S. and M.M. (Mohammadreza Mashayekhi); writing—review and editing, M.M. (Mohammadreza Mashayekhi) and D.-P.N.K.; visualization, H.S.; supervision, M.M. (Mohammadreza Mashayekhi), M.M.M., D.-P.N.K. and M.M. (Masoud Mirtaheri); project administration, D.-P.N.K. All authors have read and agreed to the published version of the manuscript.

Funding: This research received no external funding.

Data Availability Statement: The data used to support the findings of this study are included within the article.

Conflicts of Interest: The authors declare no conflicts of interest.

References

1. Buckle, I.G. *The Northridge, California Earthquake of January 17, 1994: Performance of Highway Bridges*; NCEER-94-0008; National Center for Earthquake Engineering Research: Buffalo, NY, USA, 1994.
2. Bruneau, M.; Wilson, J.C.; Tremblay, R. Performance of steel bridges during the 1995 Hyogo-ken Nanbu (Kobe, Japan) earthquake. *Can. J. Civ. Eng.* **1996**, *23*, 678–713. [CrossRef]
3. Chang, K.-C.; Chang, D.-W.; Tsai, M.-H.; Sung, Y.-C. Seismic performance of highway bridges. *Earthq. Eng. Eng. Seismol.* **2000**, *2*, 55–77.
4. Hamada, M.; Nakamura, S.; Ohsumi, T.; Megro, K.; Wang, E. *The 1999 Ji-Ji Earthquake, Taiwan-Investigation into Damage to Civil Engineering Structures*; Japan Society of Civil Engineering: Tokyo, Japan, 1999.
5. Moehle, J.P. (Ed.) *Preliminary Report on the Seismological and Engineering Aspects of the January 17, 1994 Northridge Earthquake*; Report No. UCB/EERC-94/01; Earthquake Engineering Research Center, University of California: Berkeley, CA, USA, 1994.
6. Padgett, J.E. Seismic Vulnerability Assessment of Retrofitted Bridges Using Probabilistic Methods. Ph.D. Thesis, Georgia Institute of Technology, Atlanta, GA, USA, 2007.
7. Furinghetti, M.; Reale, S.; Fox, M.J.; Pavese, A. Numerical assessment of the seismic vulnerability of bridges within the Italian road network. *Appl. Sci.* **2023**, *13*, 8194. [CrossRef]
8. Bakhshi, A.; Soltanieh, H. Development of fragility curves for existing residential steel buildings with concentrically braced frames. *Sci. Iran.* **2019**, *26*, 2212–2228.
9. Christopher, R.; Roland, L. *ATC-13: Earthquake Damage Evaluation Data for California*; Applied Technology Council: Redwood City, CA, USA, 1985.
10. Basöz, N.I.; Kiremidjian, A.S.; King, S.A.; Law, K.H. Statistical analysis of bridge damage data from the 1994 Northridge, CA, earthquake. *Earthq. Spectra* **1999**, *15*, 25–54. [CrossRef]

11. Basöz, N.I.; Kiremidjian, A.S. *Evaluation of Bridge Damage Data from the Loma Prieta and Northridge, California Earthquakes*; Rep. No. MCEER-98-0004; Multidisciplinary Center for Earthquake Engineering Research: Buffalo, NY, USA, 1998.
12. Shinozuka, M.; Kim, S.-H.; Kushiyama, S.; Yi, J.-H. Fragility curves of concrete bridges retrofitted by column jacketing. *Earthq. Eng. Eng. Vib.* **2002**, *1*, 195–205. [CrossRef]
13. Padgett, J.E.; DesRoches, R. Retrofitted bridge fragility analysis for typical classes of multispan bridges. *Earthq. Spectra* **2009**, *25*, 117–141. [CrossRef]
14. Zhang, J.; Huo, Y. Evaluating effectiveness and optimum design of isolation devices for highway bridges using the fragility function method. *Eng. Struct.* **2009**, *31*, 1648–1660. [CrossRef]
15. Agrawal, A.; Ghosn, M.; Alampalli, S.; Pan, Y. Seismic fragility of retrofitted multispan continuous steel bridges in New York. *J. Bridge Eng.* **2012**, *17*, 562–575. [CrossRef]
16. Pan, Y.; Agrawal, A.K.; Ghosn, M.; Alampalli, S. Seismic fragility of multispan simply supported steel highway bridges in New York State. II: Fragility analysis, fragility curves, and fragility surfaces. *J. Bridge Eng.* **2010**, *15*, 462–472.
17. Karimi-Moridani, K.; Zarfam, P.; Ghafory-Ashtiany, M. A novel and efficient hybrid method to develop the fragility curves of horizontally curved bridges. *KSCE J. Civ. Eng.* **2020**, *24*, 508–524. [CrossRef]
18. Yazgan, U. Empirical seismic fragility assessment with explicit modeling of spatial ground motion variability. *Eng. Struct.* **2015**, *100*, 479–489. [CrossRef]
19. Hwang, H.; Jernigan, J.B.; Lin, Y.-W. Evaluation of seismic damage to Memphis bridges and highway systems. *J. Bridge Eng.* **2000**, *5*, 322–330. [CrossRef]
20. Basoz, N.; Mander, J. *Enhancement of the Lifeline Transportation Module in HAZUS*; Report No. Draft #7; National Institute of Building Sciences: Washington, DC, USA, 1999.
21. Shinozuka, M.; Feng, M.Q.; Kim, H.-K.; Kim, S.-H. Nonlinear static procedure for fragility curve development. *J. Eng. Mech.* **2000**, *126*, 1287–1295. [CrossRef]
22. Hwang, H.; Liu, J.; Chiu, Y. *Seismic Fragility Analysis of Highway Bridges*; Report No. MAEC RR-4; Center for Earthquake Research Information: Memphis, TN, USA, 2000.
23. Shinozuka, M.; Feng, M.Q.; Lee, J.; Naganuma, T. Statistical analysis of fragility curves. *J. Eng. Mech.* **2000**, *126*, 1224–1231. [CrossRef]
24. Choi, E.; DesRoches, R.; Nielson, B. Seismic fragility of typical bridges in moderate seismic zones. *Eng. Struct.* **2004**, *26*, 187–199. [CrossRef]
25. Mackie, K.; Stojadinovic, B. Fragility curves for reinforced concrete highway overpass bridges. In Proceedings of the 13th World Conference on Earthquake Engineering, Vancouver, BC, Canada, 1–6 August 2004; Paper No. 1553.
26. Nielson, B.G.; DesRoches, R. Seismic fragility methodology for highway bridges using a component level approach. *Earthq. Eng. Struct. Dyn.* **2007**, *36*, 823–839. [CrossRef]
27. Nielson, B.G.; DesRoches, R. Analytical seismic fragility curves for typical bridges in the central and southeastern United States. *Earthq. Spectra* **2007**, *23*, 615–633. [CrossRef]
28. Avşar, Ö.; Yakut, A.; Caner, A. Analytical fragility curves for ordinary highway bridges in Turkey. *Earthq. Spectra* **2011**, *27*, 971–996. [CrossRef]
29. Tavares, D.H.; Suescun, J.R.; Paultre, P.; Padgett, J.E. Seismic fragility of a highway bridge in Quebec. *J. Bridge Eng.* **2013**, *18*, 1131–1139. [CrossRef]
30. Mackie, K.; Stojadinović, B. Comparison of incremental dynamic, cloud, and stripe methods for computing probabilistic seismic demand models. In Proceedings of the Structures Congress 2005: Metropolis and Beyond, New York, NY, USA, 20–24 April 2005.
31. Mangalathu, S.; Jeon, J.S. Stripe-based fragility analysis of multispan concrete bridge classes using machine learning techniques. *Earthq. Eng. Struct. Dyn.* **2019**, *48*, 1238–1255. [CrossRef]
32. Kiani, J.; Camp, C.; Pezeshk, S. On the application of machine learning techniques to derive seismic fragility curves. *Comput. Struct.* **2019**, *218*, 108–122. [CrossRef]
33. Bray, J.D.; Rodriguez-Marek, A. Characterization of forward-directivity ground motions in the near-fault region. *Soil Dyn. Earthq. Eng.* **2004**, *24*, 815–828. [CrossRef]
34. Mansouri, S.; Kontoni, D.-P.N.; Pouraminian, M. The effects of the duration, intensity and magnitude of far-fault earthquakes on the seismic response of RC bridges retrofitted with seismic bearings. *Adv. Bridge Eng.* **2022**, *3*, 19. [CrossRef]
35. Somerville, P. Characterizing near fault ground motion for the design and evaluation of bridges. In Proceedings of the 3rd National Seismic Conference and Workshop on Bridges and Highways, MCEER Buttalo, Portland, OR, USA, 28 April–1 May 2002.
36. Alavi, B.; Krawinkler, H. Strengthening of moment-resisting frame structures against near-fault ground motion effects. *Earthq. Eng. Struct. Dyn.* **2004**, *33*, 707–722. [CrossRef]
37. Gerami, M.; Abdollahzadeh, D. Vulnerability of steel moment-resisting frames under effects of forward directivity. *Struct. Des. Tall Spec. Build.* **2015**, *24*, 97–122. [CrossRef]
38. Yadav, K.K.; Gupta, V.K. Near-fault fling-step ground motions: Characteristics and simulation. *Soil Dyn. Earthq. Eng.* **2017**, *101*, 90–104. [CrossRef]
39. Baig, M.A.; Islam, N.; Ansari, M.I.; Umair, M. Vulnerability assessment of steel box-girder bridge under near-field and far-field earthquakes. *Innov. Infrastruct. Solut.* **2023**, *8*, 19. [CrossRef]

40. Mosleh, A.; Razzaghi, M.S.; Jara, J.; Varum, H. Seismic fragility analysis of typical pre-1990 bridges due to near-and far-field ground motions. *Int. J. Adv. Struct. Eng. (IJASE)* **2016**, *8*, 1–9. [CrossRef]
41. Billah, A.M.; Alam, M.S.; Bhuiyan, M.R. Fragility analysis of retrofitted multicolumn bridge bent subjected to near-fault and far-field ground motion. *J. Bridge Eng.* **2013**, *18*, 992–1004. [CrossRef]
42. Naseri, A.; Roshan, A.M.G.; Pahlavan, H.; Amiri, G.G. Effects of curvature radius on vulnerability of curved bridges subjected to near and far-field strong ground motions. *Struct. Monit. Maint.* **2020**, *7*, 367.
43. Chen, X. System fragility assessment of tall-pier bridges subjected to near-fault ground motions. *J. Bridge Eng.* **2020**, *25*, 04019143. [CrossRef]
44. Shao, Y.; Wei, Y.; Yang, T.; Ni, M.; Zhong, J. Empirical models of bridge seismic fragility surface considering the vertical effect of near-fault ground motions. *Structures* **2021**, *34*, 2962–2973. [CrossRef]
45. Hosseini Lavassani, S.H.; Kontoni, D.-P.N.; Alizadeh, H.; Gharehbaghi, V. Passive Control of Ultra-Span Twin-Box Girder Suspension Bridges under Vortex-Induced Vibration Using Tuned Mass Dampers: A Sensitivity Analysis. *Buildings* **2023**, *13*, 1279. [CrossRef]
46. Kontoni, D.-P.N.; Farghaly, A.A. Mitigation of the seismic response of a cable-stayed bridge with soil-structure-interaction effect using tuned mass dampers. *Struct. Eng. Mech.* **2019**, *69*, 699–712.
47. Kottegoda, N.T.; Rosso, R. *Statistics, Probability and Reliability for Civil and Environmental Engineers*; McGraw-Hill Publishing Company: New York, NY, USA, 1997.
48. Jeon, J.-S.; Mangalathu, S.; Song, J.; Desroches, R. Parameterized seismic fragility curves for curved multi-frame concrete box-girder bridges using Bayesian parameter estimation. *J. Earthq. Eng.* **2019**, *23*, 954–979. [CrossRef]
49. Cornell, C.A.; Jalayer, F.; Hamburger, R.O.; Foutch, D.A. Probabilistic basis for 2000 SAC Federal Emergency Management Agency Steel Moment Frame Guidelines. *J. Struct. Eng.* **2002**, *128*, 526–533. [CrossRef]
50. Nielson, B.G. Analytical Fragility Curves for Highway Bridges in Moderate Seismic Zones. Ph.D. Thesis, Georgia Institute of Technology, Atlanta, GA, USA, 2005.
51. Hwang, H.; Liu, J.B.; Chiu, Y.-H. *Seismic Fragility Analysis of Highway Bridges*; Mid-America Earthquake Center Technical Report MAEC RR-4 Project; Center for Earthquake Research and Information, The University of Memphis: Memphis, TN, USA, 2001.
52. McKenna, F. Open System for Earthquake Engineering Simulation (OpenSees), Version 2.4.4; MP [Software]. 2014. Available online: https://opensees.berkeley.edu/ (accessed on 10 July 2017).
53. Muthukumar, S.; DesRoches, R. A Hertz contact model with non-linear damping for pounding simulation. *Earthq. Eng. Struct. Dyn.* **2006**, *35*, 811–828. [CrossRef]
54. Caltrans. *Seismic Design Criteria*; Version 1.1; California Department of Transportation: Sacramento, CA, USA, 1999.
55. Baker, J.W. Quantitative classification of near-fault ground motions using wavelet analysis. *Bull. Seismol. Soc. Am.* **2007**, *97*, 1486–1501. [CrossRef]
56. Mallat, S.G. Multiresolution approximations and wavelet. *Trans. Am. Math. Soc.* **1989**, *315*, 69–87.
57. Haselton, C.B. Assessing Seismic Collapse Safety of Modern Reinforced Concrete Moment Frame Buildings. Ph.D. Thesis, Stanford University, Stanford, CA, USA, 2006.
58. FEMA-NIBS. *Earthquake Loss Estimation Methodology—HAZUS Technical Manual*; Federal Emergency Management Agency (FEMA) and National Institute of Building Sciences (NIBS): Washington, DC, USA, 2003.
59. FEMA. *Using HAZUS-MH for Risk Assessment—How to Guide*; FEMA 433; Federal Emergency Management Agency (FEMA): Washington, DC, USA, 2004.
60. Arora, H.C.; Kumar, S.; Kontoni, D.-P.N.; Kumar, A.; Sharma, M.; Kapoor, N.R.; Kumar, K. Axial Capacity of FRP-Reinforced Concrete Columns: Computational Intelligence-Based Prognosis for Sustainable Structures. *Buildings* **2022**, *12*, 2137. [CrossRef]
61. Hu, X.; Shentu, J.; Xie, N.; Huang, Y.; Lei, G.; Hu, H.; Guo, P.; Gong, X. Predicting triaxial compressive strength of high-temperature treated rock using machine learning techniques. *J. Rock Mech. Geotech. Eng.* **2023**, *15*, 2072–2082. [CrossRef]
62. Sharma, S.; Arora, H.C.; Kumar, A.; Kontoni, D.-P.N.; Kapoor, N.R.; Kumar, K.; Singh, A. Computational Intelligence-Based Structural Health Monitoring of Corroded and Eccentrically Loaded Reinforced Concrete Columns. *Shock Vib.* **2023**, *2023*, 9715120. [CrossRef]
63. Mirrashid, M.; Naderpour, H.; Kontoni, D.-P.N.; Jakubczyk-Gałczyńska, A.; Jankowski, R.; Nguyen, T.N. Optimized Computational Intelligence Model for Estimating the Flexural Behavior of Composite Shear Walls. *Buildings* **2023**, *13*, 2358. [CrossRef]
64. Naderpour, H.; Abbasi, M.; Kontoni, D.-P.N.; Mirrashid, M.; Ezami, N.; Savvides, A.-A. Integrating Image Processing and Machine Learning for the Non-Destructive Assessment of RC Beams Damage. *Buildings* **2024**, *14*, 214. [CrossRef]